Nevertheless, any solar phenomenon that is both long-lived and periodic may be predictable. The evidence presented here suggests that the occurrence, and perhaps the solar location, of large coronal holes could be predicted many months in advance. The established link between coronal holes and geomagnetic disturbances, and the possible link to super-active regions, raise the possibility of predicting the most important solar-induced disturbances. The existence of stability, periodicity and hemispheric asymmetry in coronal holes implies long-lived, non-random generation of magnetic flux. This will affect our understanding of the most fundamental problems in solar astrophysics, the nature of the solar cycle. □

Received 20 March; accepted 6 October 1992.

1. *Solar-Geophysical Data* (World Data Center-A for Solar-Terrestrial Physics, Boulder Colorado).
2. McIntosh, P. S. *UAG Rep.* 70 (World Data Center A for Solar-Terrestrial Physics, Boulder Colorado, 1979).
3. McIntosh, P. S. in *Solar Activity Observations and Predictions* (eds McIntosh, P. S. & Dryer, M.) 65–92 (Massachusetts Inst. Technol., 1972).
4. McIntosh, P. S. *Rev. Geophys. Space Phys.* **10,** 837–846 (1972).
5. Harvey, J. W., Krieger, A. S., Davis, J. M., Timothy, A. F. & Vaiana, G. S. *Bull. Am. astr. Soc.* **7,** 358 (1975).
6. McIntosh, P. S., Willock, E. C. & Thompson, R. J. *UAG Rep.* 101 (World Data Center A for Solar-Terrestrial Physics, Boulder Colorado, 1991).
7. Harvey, J. W. *Osserv. Mem. "Osserv Astrofis. Arcetri"*, **104,** 50–58 (1975).
8. Harvey, J. W. & Sheeley, N. R. Jr *Space Sci. Rev.* **23,** 139–158 (1979).
9. Kahler, S. W., Davis, J. M. & Harvey, J. W. *Solar Phys.* **87,** 47–56 (1983).
10. Rieger, E. *et al. Nature* **312,** 623–625 (1984).
11. Ichimoto, K., Kubota, J., Suzuki, M., Tohmura, I. & Kurokawa, H. *Nature* **316,** 422–424 (1985).
12. Bai, T. & Sturrock, P. A. *Nature* **327,** 601–604 (1987).
13. Bogart, R. S. & Bai, T. *Astrophys. J.* **299,** L51–55 (1985).
14. Thompson, R. J. & Willock, E. C. *Proc. Leura Solar Terrestrial Predictions Workshop*, Vol. 1 (eds Thompson, R. J. *et al.*), 603–610 (1990).
15. Garcia, H. A. *Solar Phys.* **127,** 185–197 (1990).
16. Hoeksema, J. T. & Scherrer, P. H. *Astrophys. J.* **318,** 428–436 (1987).
17. Hansen, R. & Hansen, S. *Solar Phys.* **44,** 225–230 (1975).
18. Verma, V. K. *Solar Phys.* **114,** 185–188 (1987).
19. Roy, J.-R. *Solar Phys.* **52,** 53–61 (1977).
20. Svalgaard, L. & Wilcox, J. M. *Solar Phys.* **41,** 461–475 (1975).
21. Sheeley, N. R. Jr, Harvey, J. W. & Feldman, W. C. *Solar Phys.* **49,** 271–278 (1976).
22. Sheeley, N. R. Jr, Harvey, J. W. *Solar Phys.* **70,** 237–249 (1981).
23. McIntosh, P. S. *EOS* **72,** 383 (1991).
24. McIntosh, P. S. in *Proc. Solar Cycle Workshop* (ed. Harvey, K.) (National Solar Observatory, Sunspot, New Mexico, in the press).
25. McIntosh, P. S. *Solar Phys.* **125,** 251–267 (1990).

ACKNOWLEDGEMENTS. We thank S. Suess for converting the analog synoptic maps into digital format, B. Paterson for assistance with Fourier analysis and D. Tranquille for assistance with the figures.

Phase behaviour of metastable water

Peter H. Poole, Francesco Sciortino, Ulrich Essmann & H. Eugene Stanley

Center for Polymer Studies and Department of Physics, Boston University, Boston, Massachusetts 02215 USA

THE metastable extension of the phase diagram of liquid water exhibits rich features that manifest themselves in the equilibrium properties of water. For example, the density maximum at 4 °C and the minimum in the isothermal compressibility at 46 °C are thought to reflect the presence of singularities in the behaviour of thermodynamic quantities occurring in the supercooled region[1,2]. The 'stability–limit conjecture'[3–5] suggests that these thermodynamic anomalies arise from a single limit of mechanical stability (spinodal line), originating at the liquid–gas critical point, which determines the limit of both superheating at high temperatures and supercooling at low temperatures. Here we present a comprehensive series of molecular dynamics simulations which suggest that, instead, the supercooling anomalies are caused by a newly identified critical point, above which the two metastable amorphous phases of ice (previously shown to be separated by a line of first-order transitions[6,7]) become indistinguishable. The two amorphous ice phases are thus incorporated into our understanding of the liquid state, providing a more complete picture of the metastable and stable behaviour of water.

The equation of state of a fluid expresses the shape of the surface $P(V, T)$ in the space of pressure P, specific volume V and temperature T. Spinodal lines on the $P(V, T)$ surface separate metastable states from those that are mechanically unstable. In practice, nucleation of a stable phase precludes study of metastable states arbitrarily close to the spinodal[8]. Many thermodynamic functions and dynamic properties of the system, however, become singular near a spinodal line in a fashion analogous to their behaviour at a critical point[9]. Hence, although the spinodal may not be attainable, its influence on nearby states can still be observed.

One well-known equilibrium anomaly of a liquid is the existence at constant P of a temperature of maximum density (TMD). As P varies, the TMD becomes a line, the TMD line.

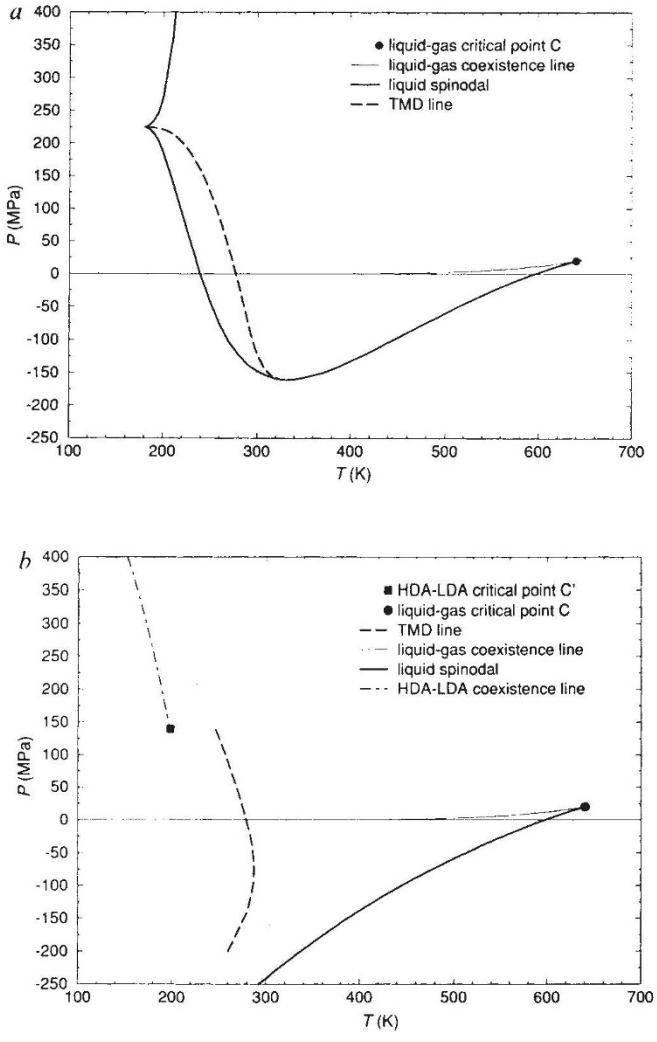

FIG. 1 *a*, The phase diagram predicted by the stability-limit conjecture[4,12], showing the TMD line intersecting a re-entrant liquid spinodal line. The liquid–gas coexistence curve ends in the liquid–gas critical point *C*. *b*, Phase diagram of ST2 water. The liquid spinodal originating at the liquid–gas critical point *C* does not intersect the TMD line. The existence of a gap between the TMD line and the spinodal implies that the anomalies are suppressed by sufficiently negative *P*, so that the region between the TMD line and the spinodal is characterized by a normal (positive) isobaric expansivity. The appearance of a TMD line with positive slope has been observed in simulations of the gaussian core model[27], a simple pair-potential unrelated to ST2. Preliminary results on the TIP4P potential indicate a similar behaviour of the TMD line. A new coexistence line, distinct from the liquid–gas coexistence line, separates two phases analogous in structure to the LDA and HDA ice phases, and ends in a critical point *C'*. The locations of the liquid spinodal and of *C'* estimated here take into account the pressure and temperature shifts of the ST2 data described in Fig. 5.

As first argued for water[4], and later[10–12] for any liquid exhibiting a TMD, there exist thermodynamic constraints on the way a spinodal and a TMD line may meet. The spinodal line $P_s(T)$ originates at the liquid–gas critical point and lies below the liquid–gas coexistence line in the P–T phase diagram (Fig. 1*a*). Experiments show[13] that $P_s(T)$ passes into the negative P region of the phase diagram. Negative P thermodynamic states are well-defined (metastable) states of hydrostatic tension, so the spinodal line at negative P represents the limit of tensile strength of the liquid. The observed TMD line of liquid water, where it

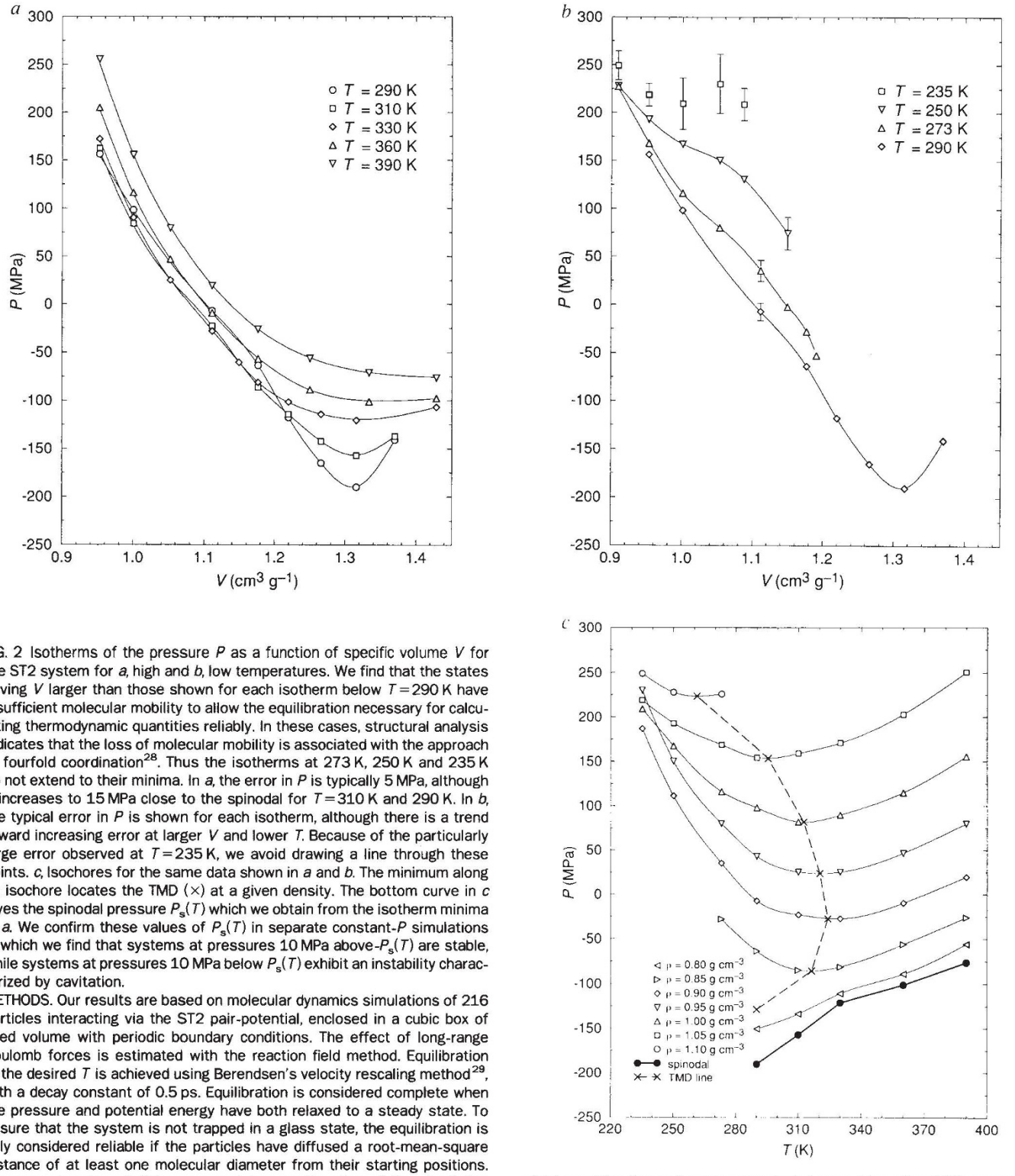

FIG. 2 Isotherms of the pressure P as a function of specific volume V for the ST2 system for *a*, high and *b*, low temperatures. We find that the states having V larger than those shown for each isotherm below $T = 290$ K have insufficient molecular mobility to allow the equilibration necessary for calculating thermodynamic quantities reliably. In these cases, structural analysis indicates that the loss of molecular mobility is associated with the approach to fourfold coordination[28]. Thus the isotherms at 273 K, 250 K and 235 K do not extend to their minima. In *a*, the error in P is typically 5 MPa, although it increases to 15 MPa close to the spinodal for $T = 310$ K and 290 K. In *b*, the typical error in P is shown for each isotherm, although there is a trend toward increasing error at larger V and lower T. Because of the particularly large error observed at $T = 235$ K, we avoid drawing a line through these points. *c*, Isochores for the same data shown in *a* and *b*. The minimum along an isochore locates the TMD (×) at a given density. The bottom curve in *c* gives the spinodal pressure $P_s(T)$ which we obtain from the isotherm minima in *a*. We confirm these values of $P_s(T)$ in separate constant-P simulations in which we find that systems at pressures 10 MPa above-$P_s(T)$ are stable, while systems at pressures 10 MPa below $P_s(T)$ exhibit an instability characterized by cavitation.

METHODS. Our results are based on molecular dynamics simulations of 216 particles interacting via the ST2 pair-potential, enclosed in a cubic box of fixed volume with periodic boundary conditions. The effect of long-range Coulomb forces is estimated with the reaction field method. Equilibration to the desired T is achieved using Berendsen's velocity rescaling method[29], with a decay constant of 0.5 ps. Equilibration is considered complete when the pressure and potential energy have both relaxed to a steady state. To ensure that the system is not trapped in a glass state, the equilibration is only considered reliable if the particles have diffused a root-mean-square distance of at least one molecular diameter from their starting positions. The average value of P is measured in a continuation of the simulation after equilibration, in which T is controlled with Berendsen's method, and confirmed in further constant-(N, V, E) simulations. The time step for the update of particle positions is fixed at 1.0 fs. In almost all cases, a given simulation is started using the final particle positions of a previous simulation at a state point as near as possible to the new one. The lengths of the runs (equilibration plus production) vary depending on the time needed to obtain equilibration and measurements, but are not less than 200 ps except at the highest T. Because of the slow relaxation found in the systems at the lowest T and highest specific volumes, run times of 600 to 800 ps are typical in this regime. To confirm that the behaviour we find near the spinodal is not an artefact of the small system size, we have reproduced the position and shape of the $\rho = 0.80\ \mathrm{g\,cm^{-3}}$ isochore shown in *c* in constant P simulations of a system of 1,728 ST2 particles.

has been measured[14], has negative slope, and would intersect the spinodal line at negative P if this trend were to continue. But the thermodynamic constraints on the intersection of spinodal and TMD lines demand[10–12] that $P_s(T)$ passes through a minimum at this intersection point; $P_s(T)$ moves back to higher P as T is further lowered, and eventually becomes positive at sufficiently low T (Fig. 1*a*). The stability-limit conjecture states that such a 're-entrant' spinodal actually occurs in liquid water, and moreover gives rise to the anomalous behaviour of this liquid at low T. Note that this hypothesis requires that a spinodal line $P_s(T)$ always has negative slope in the T range of the phase diagram in which a TMD line is found.

We initially sought to discover the extent to which the stability-limit conjecture (represented by Fig. 1*a*) is borne out in molecular dynamics computer simulation, but in fact we find that our results suggest a rather different phase diagram (Fig. 1*b*). In the present simulations, we use the ST2 potential[15] to calculate the interparticle interactions because, out of the potentials that we tested (TIP4P[16], SPC/E[17] and ST2), ST2 exhibits the best developed density maximum. Additionally, the range of temperature between the TMD and the lowest temperature that can be studied (beyond which there is insufficient molecular mobility) is much larger for ST2 than for the other potentials. Thus ST2 water can be studied deep into the anomalous region.

We locate the spinodal $P_s(T_0)$, for a fixed temperature T_0, from the $T = T_0$ isotherm in a plot of P against V as the point for which the pressure is a minimum (Fig. 2*a*). This is equivalent to the condition that the isothermal compressibility $K_T = -1/V(\partial V/\partial P)_T$ becomes singular.

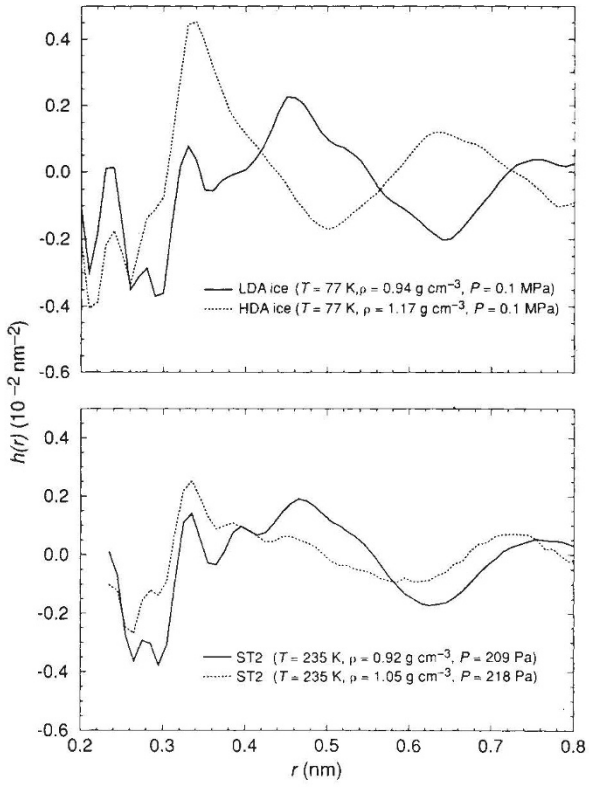

FIG. 3 Plots of the neutron-weighted pair correlation function $h(r)$ as determined in experiment[19] at $T = 77$ K for the HDA and LDA ices (top panel) compared with the ST2 system at 235 K at two values of density straddling the critical density (bottom panel). Here $h(r)$ is defined in terms of the radial distribution functions $g_{O\text{-}O}(r)$, $g_{O\text{-}H}(r)$ and $g_{H\text{-}H}(r)$, which give the probabilities that an atom of a particular type is in a differential radial distance element dr at a distance r from a given atom: $h(r) = 4\pi\rho r(0.092g_{O\text{-}O}(r) + 0.422g_{O\text{-}H}(r) + 0.486g_{H\text{-}H}(r) - 1)$, where the coefficients are appropriate for neutron scattering experiments[30], O refers to oxygen, and H to hydrogen.

Unexpectedly, we find that the spinodal is a monotonic function of T and thus is not re-entrant (a result confirmed independently[18]), even at temperatures below those at which a TMD is observed (Fig. 2*c*). Such behaviour, although different from the stability-limit conjecture, is nonetheless thermodynamically consistent. The TMD line, although it has negative slope at high P, acquires a positive slope at low P, thereby avoiding an intersection with the spinodal, and thus pre-empting a re-entrant spinodal. The assumption made in the stability-limit conjecture, that the TMD line has negative slope throughout the phase diagram, is therefore not borne out by our calculations (Fig. 2*c*).

If there is no re-entrant spinodal, then what causes the known anomalous behaviour of water? Our calculations suggest that the cause is a novel critical point C', which is unrelated to the liquid–gas critical point C. The evidence is four-fold:

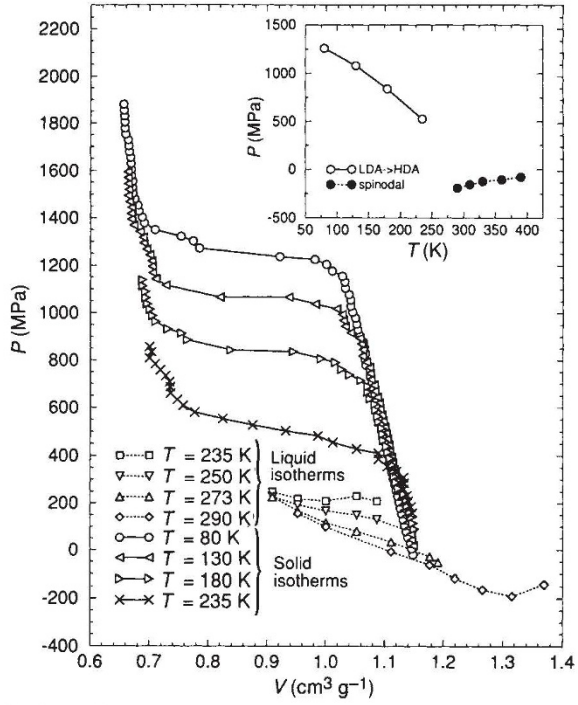

FIG. 4 Isothermal compression curves for the low-density amorphous solid ST2 system. For comparison, the low-temperature ST2 liquid isotherms are reproduced from Fig. 2*b*. We simulate the isothermal compression employed in the experiments by monitoring the specific volume of the system during a simulation in which T and P are controlled with Berensen's method, and in which P is increased stepwise. A similar simulation procedure[31] has been successful in reproducing the experimentally observed[6] P-induced transition from ice I_h to HDA ice. We apply this procedure to LDA ice obtained by cooling the simulated low density liquid to below $T_{C'}$. The inset shows the pressures (○) of the inflections in the isothermal compression curves as a function of T, in relation to the location of the liquid spinodal of Fig. 2*c*. The isothermal compression curves are generated in the following way: the equilibrated system configuration obtained from the simulation at $\rho = 0.87$ g cm^{-3}, $T = 250$ K is cooled for a period of 180 ps at constant V to 200 K, and then for another 50 ps to each of several different temperatures, $T = 80$ K, 130 K, 180 K and 235 K. Each of these systems is then used as the initial (LDA ice-like) configuration for a constant-P, constant-T simulation, beginning at the nominal P and T resulting from the cooling procedure. During the simulation, P is increased in increments of 25 MPa every 10 ps, while T is maintained via Berendsen's method of velocity rescaling with relaxation time 0.5 ps. To check this result, we found that simulations using different starting configurations, P increments of 50 MPa every 10 ps, or P increments of 25 MPa every 20 ps, do not give significantly different results. These isothermal compressions represent non-equilibrium processes, because the systems are at too low a temperature to have time to relax to equilibrium within the stated simulation scheme. The $T = 235$ K run therefore serves as a check on the deviation induced by pushing the system kinetically through an entire isotherm. As seen in this figure, there is a ~200 MPa pressure gap between the $T = 235$ K isothermal compression run, and the equilibrium simulation points at the same T.

(1) The low-temperature isotherms (Fig. 2*b*) show an intriguing trend: each exhibits an inflection in the region around a density $\rho = 1.00\ \mathrm{g\ cm^{-3}}$ which increases in strength as T is decreased. The shape and T dependence of these inflections are similar to what would occur for isotherms if a critical point were approached from above in T.

(2) The existence of a critical point C' would imply the onset of a two-phase coexistence region, so we next explore the two phases that must become distinct below C'. The structure of the system at densities just above and just below the estimated critical density $\rho_{C'} = 1.00\ \mathrm{g\ cm^{-3}}$ is reflected in Fig. 3, which shows the pair correlation function $h(r)$ at a temperature close to the estimated critical temperature $T_{C'}$. Our calculations are compared with the experimentally measured $h(r)$ for the two amorphous ice phases, high-density amorphous ice (HDA) and low-density amorphous ice (LDA)[19]. The similarity between $h(r)$ for the HDA phase and our ST2 calculations just above $\rho_{C'}$ as well as the similarity between the LDA phase and our ST2 calculations just below $\rho_{C'}$ supports the possibility that C' is a critical point for a phase transition between a HDA-like substance and an LDA-like substance. Indeed, the fact that the two phases are both amorphous allows the possibility of a second-order transition.

(3) The phase transition from LDA to HDA ice has been observed in isothermal compression experiments[7] at 77 K. If C' were the critical point of the LDA–HDA ice transition in ST2 water, then simulated isothermal compressions of the ST2 system at temperatures below $T_{C'}$ should reproduce this LDA–HDA ice transition. The isothermal compression curves for temperatures below $T_{C'}$ are shown in Fig. 4. The analogue of the LDA–HDA transition is indicated by the sharp inflections in the isotherms, which are plausibly continuous with those generated from the liquid-state simulations. Our confidence in the reliability of conclusions drawn from the ST2 potential is enhanced by our finding that ST2 can reproduce the experimentally observed LDA–HDA transition.

(4) To confirm that the phase behaviour, reflected in Fig. 1*b*, is consistent with experimental results, we compare in Fig. 5 the T dependence of density, K_T, and isobaric specific heat at ambient pressure.

Before concluding, we note that our ST2 calculations lead to an overall phase diagram of the generic form displayed in Fig. 1*b*. The slope of the TMD line changes sign at low pressures, avoiding an intersection with the liquid spinodal, and the possibility of re-entrance of this spinodal. The HDA/LDA

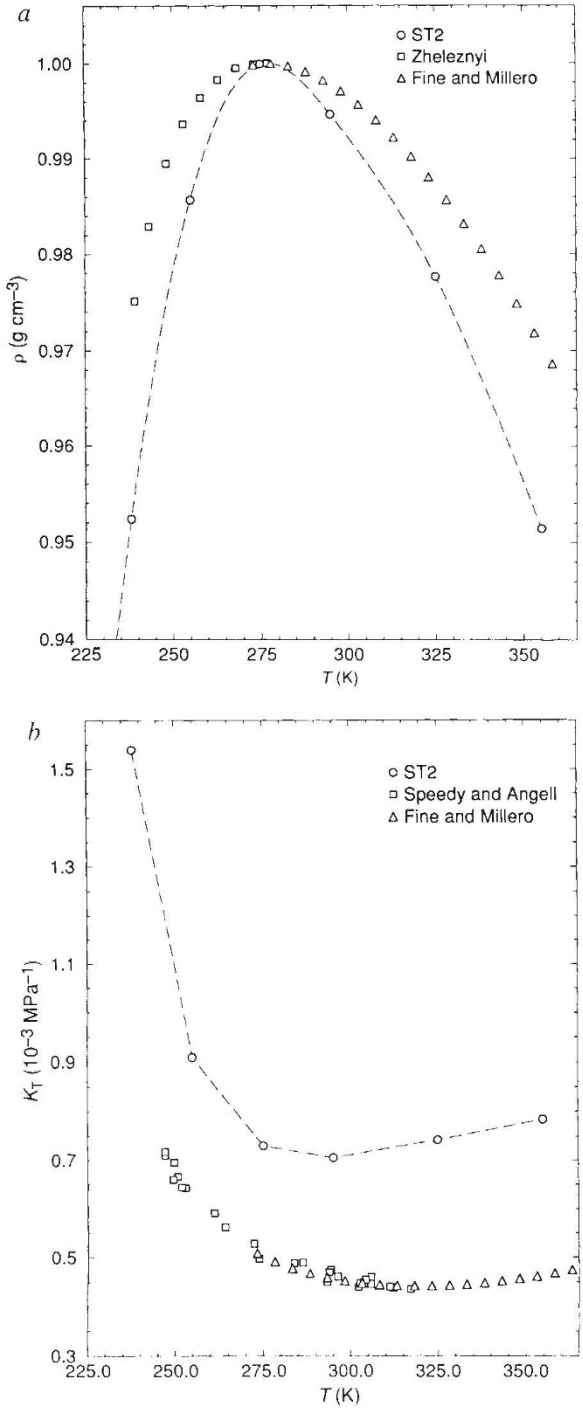

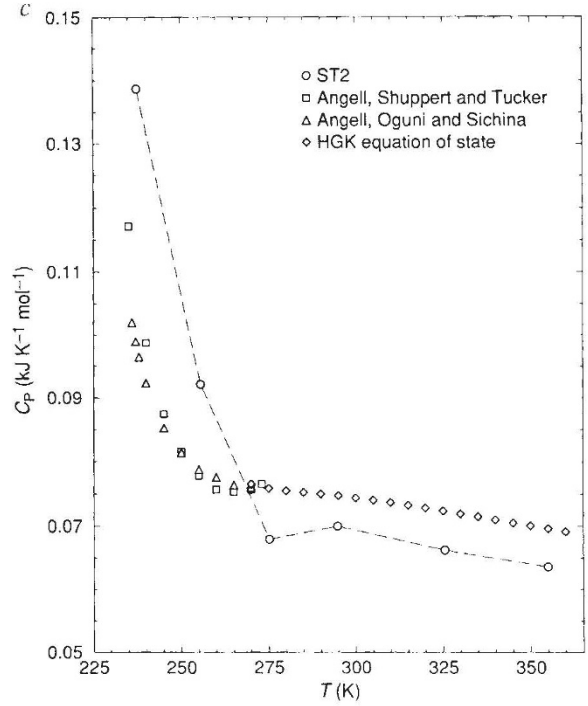

FIG. 5 Comparison between experiment and our ST2 calculations for (*a*) the density ρ, (*b*) the isothermal compressibility K_T, and (*c*) the isobaric specific heat C_P. The curve in *a* through the ST2 data is a spline. Because ST2 gives the TMD for density $\rho = 1.00\ \mathrm{g\ cm^{-3}}$ at ($T = 312$ K, $P = 82$ MPa) rather than the actual values[32] of ($T = 277$ K, $P = 0.1$ MPa), for all three plots we have shifted the pressure and temperature of the ST2 properties shown by −35 K and −82 MPa to bring their respective density maxima into coincidence. The ST2 potential gives a more pronounced density maximum than for real water. Figure 4*b* and *c* demonstrates how well ST2 mimics the accelerating increases of two response functions, the isothermal compressibility[3,33] and the isobaric specific heat[1,21]. The experimental data are shown together with points obtained from the HGK equation of state[34]. The values of K_T and C_P are estimated from bicubic spline interpolations of the $P(V, T)$ and potential energy $U(V, T)$ simulation data sets.

coexistence line ending in C' has negative slope for the same reason that the coexistence line separating ice I_h and liquid water has negative slope: both the density and entropy of the lower-temperature phase are smaller than those of the higher-temperature phase[20]. There are several important implications of Fig. 1*b* for our understanding of amorphous ice and liquid water. First, the appearance of the critical point C' in supercooled water and that of the density maximum are intimately related. The isotherm inflections (Fig. 2*b*) that eventually develop into the critical point C' represent a behaviour that simultaneously allows for the increase of P along an isochore as T is lowered, a basic signature of an anomalous liquid. Second, the behaviour that we find is consistent with suggestions[21–23] that the development of a random tetrahedral network as the temperature of the liquid is lowered could occur as some sort of phase transition. Third, both amorphous ice phases are incorporated into our understanding of the liquid state, a subject of recent debate[24,25]. Specifically, we predict that LDA ice is continuously connected to the liquid by any thermodynamic path that avoids the line of first-order transitions ending at C'. Finally, the phase behaviour proposed here may be important for understanding the properties of water in confined geometries, where behaviour similar to that of the bulk liquid is exhibited, but at comparatively higher temperatures[26], thereby allowing the bulk phenomena occurring deep in the metastable region to be more readily observed. □

Received 29 July; accepted 13 October 1992.

1. Angell, C. A. in *Water: A Comprehensive Treatise* (ed. Franks, F.) Vol. 7, 1–81 (Plenum, New York, 1982).
2. Lang, E. W. & Lüdemann, H.-D. *Angew. Chem. int. Ed. Engl.* **21,** 315–329 (1982).
3. Speedy, R. J. & Angell, C. A. *J. chem. Phys.* **65,** 851–858 (1976).
4. Speedy, R. J. *J. Phys. Chem.* **86,** 982–991 (1982).
5. Speedy, R. J. *J. phys. Chem.* **86,** 3002–3005 (1982).
6. Mishima, O., Calvert, L. D. & Whalley, E. *Nature* **310,** 393–395 (1984).
7. Mishima, O., Calvert, L. D. & Whalley, E. *Nature* **314,** 76–78 (1985).
8. Gunton, J. D., San Miguel, M. & Sahni, P. S. in *Phase Transitions and Critical Phenomena* (eds Domb, C. & Lebowitz, J. L.) 267–482 (Academic, London, 1983).
9. Compagner, A. *Physica* **72,** 115–122 (1974).
10. Debenedetti, P. G. & D'Antonio, M. C. *J. chem. Phys.* **84,** 3339–3345 (1986).
11. Debenedetti, P. G. & D'Antonio, M. C. *Am. Inst. chem. Eng. J.* **34,** 447–455 (1988).
12. Debenedetti, P. G., Raghaven, V. S. & Borick, S. S. *J. phys. Chem.* **95,** 4540–4551 (1991).
13. Green, J. L., Durben, D. J., Wolf, G. H. & Angell, C. A. *Science* **249,** 649–652 (1990).
14. Henderson, S. J. & Speedy, R. J. *J. phys. Chem.* **91,** 3062–3068 (1987).
15. Stillinger, F. H. & Rahman, A. *J. chem. Phys.* **60,** 1545–1557 (1974).
16. Jorgensen, W. L., Chandrasekhar, J., Madura, J. D., Impey, R. W. & Klein, M. L. *J. chem. Phys.* **79,** 926–935 (1983).
17. Berendsen, H. J. C., Grigera, J. R. & Straatsma, T. P. *J. phys. Chem.* **91,** 6269–6271 (1987).
18. Striemann, L. thesis, Univ. of Dortmund (1992).
19. Bellissent-Funel, M.-C., Teixeira, J. & Bosio, L. *J. chem. Phys.* **87,** 2231–2235 (1987).
20. Whalley, E., Klug, D. D. & Handa, Y. P. *Nature* **342,** 782–783 (1989).
21. Angell, C. A., Shuppert, J. & Tucker, J. C. *J. phys. Chem.* **77,** 3092–3099 (1973).
22. Stanley, H. E. & Teixeira, J. *J. chem. Phys.* **73,** 3404–3422 (1980).
23. Sciortino, F., Poole, P., Stanley, H. E. & Havlin, S. *Phys. Rev. Lett.* **64,** 1686–1689 (1990).
24. Hallbrucker, A., Mayer, E. & Johari, G. P. *Phil. Mag.* **B60,** 179–187 (1989).
25. Speedy, R. J. *J. phys. Chem.* **96,** 2322–2325 (1992).
26. Dore, J. in *Correlations and Connectivity* (eds Stanley, H. E. & Ostrowsky, N.) 188–197 (Kluwer, Dordrecht, 1990).
27. Stillinger, F. H. & Weber, T. A. *J. chem. Phys.* **68,** 3837–3844 (1978).
28. Sciortino, F., Geiger, A. & Stanley, H. E. *Nature* **354,** 218–221 (1991).
29. Berendsen, H. J. C., Postma, J. P. M., van Gunsteren, W. F., DiNola, A. & Haak, J. R. *J. phys. Chem.* **81,** 3684–3690 (1984).
30. Chowdhury, M. R., Dore, J. C. & Wenzel, J. T. *J. non-cryst. Solids* **53,** 247–265 (1982).
31. Tse, J. S. & Klein, M. L. *Phys. Rev. Lett.* **58,** 1672–1675 (1987).
32. Zhelezni, B. V. *Russ. J. phys. Chem.* **43,** 1311–1312 (1969).
33. Fine, R. A. & Millero, F. J. *J. chem. Phys.* **59,** 5529–5536 (1973).
34. Haar, L., Gallagher, J. S. & Kell, G. *NBS/NRC Steam Tables* (Hemisphere, Washington DC, 1985).

ACKNOWLEDGEMENTS. We thank A. Geiger, S. C. Glotzer, S. Schwarzer and especially C. A. Angell and S. Sastry for discussions and suggestions on the manuscript, and L. Striemann for sharing his preliminary results. This work was supported by the NSF, ONR and BP.

Solar cycle length, greenhouse forcing and global climate

P. M. Kelly & T. M. L. Wigley

Climatic Research Unit, University of East Anglia, Norwich NR4 7TJ, UK

THE recent rise in global-mean surface air temperature is widely thought to be the result of increasing atmospheric concentrations of greenhouse gases[1–3], but there are discrepancies between the predicted response of the atmosphere to this radiative forcing and the observed temperature changes[1–5]. Solar irradiance fluctuations have been proposed as a possible explanation for these discrepancies, and various solar properties (for example, radius[6], smoothed sunspot number[7] or cycle length[8]) have been suggested as proxies for solar irradiance variations in the absence of direct data. Here we model the effects of a combination of greenhouse and solar-cycle-length forcing and compare the results with observed temperatures. We find that this forcing combination can explain many features of the temperature record, although the results must be interpreted cautiously; even with optimized solar forcing, most of the recent warming trend is explained by greenhouse forcing.

We use an upwelling-diffusion energy-balance climate model[4,5] to simulate the effects of greenhouse and solar forcing over the period 1765 to 1985. In a series of analyses, we vary the climate sensitivity and a scaling factor linking changes in solar cycle length to radiative forcing, and determine the best fit between annual modelled and observed global-mean (land-plus-marine) temperature[9,10] by maximizing the explained variance over the period 1861–1985 (following ref. 11).

We use two records of greenhouse forcing and allied effects. The first, 'history 1', is taken from ref. 12. The second, 'history 2', has been derived by Wigley and Raper (their 'middle' aerosol forcing case)[13] on the basis of a recent re-evaluation of the forcing associated with, *inter alia*, ozone depletion and sulphur dioxide emissions[14]. The climate sensitivity is specified by the equilibrium global-mean warming for a change in forcing (of any origin) equivalent to a doubling of the CO_2 concentration, $\Delta T_{2\times}$, and is allowed to vary between 0.5 and 5.5 °C. This exceeds the range of uncertainty associated with cloud feedback and other processes, 1.5 to 4.5 °C, based on general circulation model calculations[1]. We assume a simple linear relationship between irradiance and cycle length, consistent with ref. 8. The solar forcing term is defined by $\Delta Q_s = \beta \Delta L$, where ΔQ_s is the solar forcing change at the top of the troposphere, ΔL refers to the series of cycle-length departures from the 1765–1985 mean and β is a solar forcing scaling factor ($W m^{-2} yr^{-1}$). β is varied between −1.0 and +0.5 which implies a range of −3 to +2 $W m^{-2}$ for ΔQ_s (−1.3 to +0.8% irradiance change). We make use of

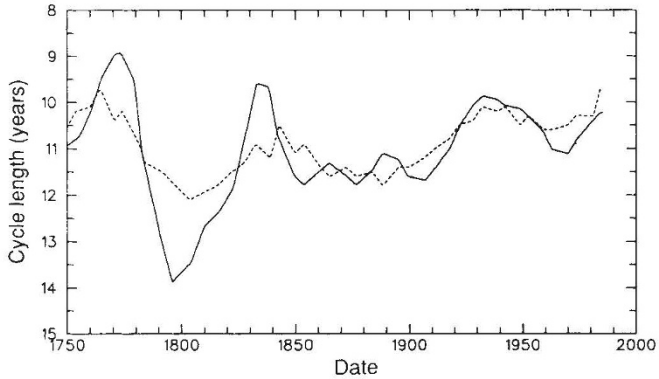

FIG. 1 The two solar cycle length records. Solid line: record derived in this paper (KW). Dashed line: record derived by Friis-Christensen and Lassen[8] (FCL). KW is derived from the same basic sunspot data set as FCL but the raw maximum-to-maximum and minimum-to-minimum length series were combined into a single series before applying a 7-term binomial filter. Differences between the records arise mainly because of the different bandwidths of the filters used. We have used the FCL record as published, although we found that they omitted two minor troughs around 1800 and that a different length for the final solar cycle is obtained when making use of the most recently available data.